

Efficient Curvature Estimation for Oriented Point Clouds

Yueqi Cao ¹, Didong Li ², Huafei Sun¹, Amir H Assadi³ and Shiqiang Zhang¹

¹*School of Mathematics and Statistics, Beijing Institute of Technology, Beijing, China*

²*Department of Mathematics, Duke University, Durham, North Carolina, United States of America*

³*Department of Mathematics, University of Wisconsin Madison, Madison, Wisconsin, United States of America*

Abstract

There is an immense literature focused on estimating the curvature of an unknown surface from point cloud dataset. Most existing algorithms estimate the curvature indirectly, that is, to estimate the surface locally by some basis functions and then calculate the curvature of such surface as an estimate of the curvature. Recently several methods have been proposed to estimate the curvature directly. However, these algorithms lack of theoretical guarantee on estimation error on small to moderate datasets. In this paper, we propose a direct and efficient method to estimate the curvature for oriented point cloud data without any surface approximation. In fact, we estimate the Weingarten map using a least square method, so that Gaussian curvature, mean curvature and principal curvatures can be obtained automatically from the Weingarten map. We show the convergence rate of our Weingarten Map Estimation (WME) algorithm is $n^{-2/3}$ both theoretically and numerically. Finally, we apply our method to point cloud simplification and surface reconstruction.

1 Introduction

Efficient estimation of (Gaussian/mean/principal) curvature for point cloud data is an important but difficult problem. In geometry, curvature contains much information of the underlying space of an unordered point set. Therefore it provides prior information in many applications such as surface segmentation [25, 34], surface reconstruction [2, 31, 33], shape inference [4, 30], point cloud simplification [12, 24] and feature extraction [11]. However, methods used to estimate curvature are restricted. Direct computation on point clouds often requires local parametrization. One needs to fit a local parametric surface first. Then the curvature is obtained by substituting the coefficients into an analytical formula. Another way is to estimate curvature after surface reconstruction which turns point clouds into triangular meshes or level sets of some distance function [10, 15, 18, 28]. However, there is little theory about estimation error analysis like convergence rate. This is not surprising since these existing algorithms are not aiming at minimizing the estimation error of the curvature, but instead to minimize the error of the

surface approximation. Note that even when surfaces are close to each other under the Euclidean distance, their curvatures might not be close to each other. For example, we can perturb a straight line a little bit so that the curvature is far away from zero. As a result, a more direct and efficient approach with theoretical guarantee on the estimation error is needed.

1.1 Related Works

Recently several methods have been proposed to directly estimate the curvature of point clouds. In [19], the authors introduced the definition of Voronoi covariance measure (VCM) to estimate the curvature for noisy point clouds. Though a stability theorem is proved, there is no assertion on convergence rate. Another class of methods is to estimate the shape operator (or Weingarten map). These methods are mainly motivated by curvature estimation techniques in triangle meshes. In the classic paper [32], G. Taubin defined a matrix by an integration formula. As illustrated in [13], this is nothing but the Weingarten map. This formula is adopted by [13] to estimate the principal curvature on point sets. The authors then proposed a method for anisotropic fairing of a point sampled surface using mean curvature flow. A similar class of methods is to estimate the second fundamental form. For example, S. Rusinkiewicz approximated the second fundamental form per triangle for meshes [27]. J. Berkmann and T. Caelli proposed two covariance matrices to approximate the second fundamental form [3]. One should be cautious to distinguish the second fundamental form and Weingarten map under general cases. Only when an orthonormal basis is chosen will the two matrices coincide.

1.2 Our Contribution

Unlike [3, 13, 32], we use differentiation formula but not integration formula to approximate Weingarten map. The core idea is to use Gauss map. Gauss map is a crucial concept in classical differential geometry of surfaces. By definition, Gauss map sends each point on a surface to its unit normal vector. For an oriented point cloud, which we mean a point cloud with a given unit normal vector field, Gauss map is automatically defined. The Gaussian/mean/principal curvatures are the determinant/trace/eigenvalues of the differential of Gauss map. Therefore, the problem of estimating curvature descends down to the estimation of the tangent map. We propose a least-square based algorithm to estimate the tangent map, with a closed form solution that is easy to compute. A statistical model is set up for error estimation and the mean square error (MSE) for matrix estimation is of order $O(n^{-2/3})$ given by the main theorem, where n is the sample size.

The convergence rate is verified by numerical experiments on two synthetic data sets. We also compare WME with the traditional quadratic fitting method, the state-of-art algorithm in this literature. Our method yields better results than the quadratic fitting in both MSE and robustness. As an application, we propose a curvature-based clustering method in point cloud simplification. Furthermore, we reconstruct surfaces based on the

simplified point clouds to give a visible comparison. Three real data sets are tested to show the gain of our WME algorithm.

1.3 Outlines

This paper is organized as follows. We introduce our WME method in section 2 followed by a statistical model to analyze the estimation error in section 3. In section 4, we verify the convergence rate and compare our method with quadratic surface fitting method using synthetic data. Applications to brain cortical data and experiments on point cloud simplification are given in section 5. In section 6, we discuss the generalizations of WME and some future works.

2 WME Algorithm

Let \mathcal{M} be a two dimensional manifold embedded in \mathbb{R}^3 . Let \mathbf{n} be a smooth unit normal vector field on \mathcal{M} . *Gauss map* sends each point $p \in \mathcal{M}$ to its unit normal vector \mathbf{n}_p .

$$\begin{aligned} \mathbf{g} : \mathcal{M} &\rightarrow \mathbb{S}^2 \\ p &\mapsto \mathbf{n}_p \end{aligned} \tag{2.1}$$

Suppose $T_p\mathcal{M}$ is the tangent space at p . The differential of the Gauss map at p is a self-adjoint operator on the tangent space $d\mathbf{g}_p : T_p\mathcal{M} \rightarrow T_p\mathcal{M}$. In convention, the operator $-d\mathbf{g}$ is called *shape operator* or *Weingarten map*. More importantly, curvatures are determined by such Weingarten map. To be more specific, the Gaussian curvature is $\det(-d\mathbf{g}_p)$, the mean curvature is $\text{Trace}(-d\mathbf{g}_p)/2$, and the principal curvatures are two eigenvalues of $-d\mathbf{g}_p$. Therefore, it suffices to estimate the Weingarten map $-d\mathbf{g}_p$.

Intuitively, the tangent map can be computed in a way analogous to the usual derivative of a function $y = f(x)$. We approximate the derivative by the difference quotient ' $\Delta y / \Delta x$ '. But there are problems when using this analogy. First, there are no natural coordinates on a surface. Thus, we cannot use numerical methods as we do for usual functions. Secondly, the tangent map is a linear operator on $T_p\mathcal{M}$, which cannot be solved by simply taking the 'ratio'. However, these two problems are not unsolvable, as we will illustrate in the following.

For the first problem, we present a coordinate-free formula for $d\mathbf{g}_p$. This can be regarded as the Taylor expansion for Gauss map at p . Denote the position vector at p by \mathbf{r}_p and the normal vector at p by \mathbf{n}_p . Let q be a point near p so that q lies in the geodesic ball centered at p . The difference of position vectors $\Delta\mathbf{r} = \mathbf{r}_q - \mathbf{r}_p$ and the difference of normal vectors $\Delta\mathbf{n} = \mathbf{n}_q - \mathbf{n}_p$ are related by the differential of Gauss map.

Proposition. Let $^\perp : \mathbb{R}^3 \rightarrow T_p\mathcal{M}$ be the orthogonal projection to $T_p\mathcal{M}$. Then

$$\Delta\mathbf{n}^\perp = d\mathbf{g}_p(\Delta\mathbf{r}^\perp) + O(\|\Delta\mathbf{r}\|^2), \tag{2.2}$$

where $\|\cdot\|$ denotes the usual Euclidean norm.

Proof. Choose a local parametrization (u, v) for \mathcal{M} around p . Assume $p = \mathbf{r}(0, 0)$ and $q = \mathbf{r}(u, v)$. Note that $\mathbf{n} = \frac{\partial \mathbf{r}}{\partial u} \times \frac{\partial \mathbf{r}}{\partial v} / \|\frac{\partial \mathbf{r}}{\partial u} \times \frac{\partial \mathbf{r}}{\partial v}\|$ is the unit normal vector field. The expansion of $\mathbf{n}(u, v)$ at $\mathbf{n}(0, 0)$ is

$$\begin{aligned} \mathbf{n}(u, v) = & (1 + O(u^2 + v^2))\mathbf{n}(0, 0) \\ & + (u + O(u^2 + v^2))\mathbf{n}_u(0, 0) + (v + O(u^2 + v^2))\mathbf{n}_v(0, 0). \end{aligned} \quad (2.3)$$

By definition of \mathbf{dg}_p , we have $\mathbf{n}_u(0, 0) = \mathbf{dg}_p(\mathbf{r}_u(0, 0))$ and $\mathbf{n}_v(0, 0) = \mathbf{dg}_p(\mathbf{r}_v(0, 0))$. Substituting them into (2.3), we have

$$\begin{aligned} \Delta \mathbf{n}^\perp(u, v) = & (u + O(u^2 + v^2))\mathbf{n}_u(0, 0) + (v + O(u^2 + v^2))\mathbf{n}_v(0, 0) \\ = & \mathbf{dg}_p((u + O(u^2 + v^2))\mathbf{r}_u(0, 0) + (v + O(u^2 + v^2))\mathbf{r}_v(0, 0)) \\ = & \mathbf{dg}_p(\Delta \mathbf{r}^\perp(u, v)) + O(u^2 + v^2). \end{aligned} \quad (2.4)$$

Note that $\|\Delta \mathbf{r}(u, v)\|^2 / (u^2 + v^2)$ is bounded, hence $O(u^2 + v^2) = O(\|\Delta \mathbf{r}(u, v)\|^2)$, and (2.2) follows. \square

Fix an orthonormal basis $\{\mathbf{e}_1, \mathbf{e}_2\}$ for $T_p\mathcal{M}$. Suppose the matrix representation of \mathbf{dg}_p under $\mathbf{e}_1, \mathbf{e}_2$ is G , i.e.

$$\mathbf{dg}_p[\mathbf{e}_1, \mathbf{e}_2] = [\mathbf{e}_1, \mathbf{e}_2]G. \quad (2.5)$$

According to the proposition, we have

$$\begin{bmatrix} \Delta \mathbf{n} \cdot \mathbf{e}_1 \\ \Delta \mathbf{n} \cdot \mathbf{e}_2 \end{bmatrix} = G \begin{bmatrix} \Delta \mathbf{r} \cdot \mathbf{e}_1 \\ \Delta \mathbf{r} \cdot \mathbf{e}_2 \end{bmatrix} + O(\|\Delta \mathbf{r}\|^2). \quad (2.6)$$

Suppose $\{P_i\}_{i=1}^n$ is a point cloud sampled from a smooth surface \mathcal{M} . Each P_i is a position vector in \mathbb{R}^3 . $\{N_i\}_{i=1}^n$ is a set consisting of outward (or inward) unit normal vectors. Let P be an arbitrary point and N be the normal vector at P . Thus, the tangent space at P is the orthogonal complement of N . Extend N to an orthonormal basis $\{E_1, E_2, N\}$ in \mathbb{R}^3 . Thus $\{E_1, E_2\}$ is the orthonormal basis in the tangent space. Without loss of generality, assume P_1, P_2, \dots, P_k are k -nearest neighbors of P . Set

$$\Delta P = [P_1 - P, P_2 - P, \dots, P_k - P]. \quad (2.7)$$

The projections of ΔP to the tangent space is given by the matrix $A = \Delta P^t [E_1, E_2]$, where t denotes the transpose of matrices. Similarly, set

$$\Delta N = [N_1 - N, N_2 - N, \dots, N_k - N]. \quad (2.8)$$

The projections of ΔN to the tangent space is given by $B = \Delta N^t [E_1, E_2]$. From (2.6), we have $B = AG + O(\|A\|^2)$. We want to minimize the residual $\|B - AG\|^2$. Consider the following optimization problem

$$\arg \min_{G \in \mathbb{R}^{2 \times 2}} \|B - AG\|^2. \quad (2.9)$$

If $A^t A$ is of full rank, The solution of (2.9) is given in the closed form

$$G = (A^t A)^{-1} A^t B. \quad (2.10)$$

If $A^t A$ is singular, the solution of (2.9) can also be given in terms of the pseudo-inverse of $A^t A$. One can also add a correction term ϵI to make it invertible. Nevertheless, for our situation, since usually $k \gg 2$, $A^t A$ is always considered to be invertible.

Now that G is given, the Gaussian curvature at P is $K = \det(-G)$, and the mean curvature is given by $H = \text{trace}(-G)/2$. Furthermore, suppose the diagonalization of G is $G = Q^{-1} \text{diag}\{\lambda_1, \lambda_2\} Q$ where Q is an orthogonal matrix, then the principal curvatures are given by $-\lambda_1$ and $-\lambda_2$, and the corresponding principal directions are given by $[e_1, e_2] Q^{-1}$.

Remark. Since the Weingarten map is a self-adjoint operator on $T_p \mathcal{M}$, the matrix G should be symmetric. It is natural to solve 2.9 on the space of symmetric matrices. However, as we will prove later, the solution of 2.9 converges to the true matrix. Since we are interested in determinants and traces, which are continuous functions of matrices, it is not necessary to solve a more complex optimization problem on the space of symmetric matrices.

3 Error Estimation

3.1 Modeling

Let Π be a distribution on the surface \mathcal{M} which is oriented by a unit normal vector field \mathbf{n} . For any $p \in \mathcal{M}$, consider the map

$$\begin{aligned} \nu_p : \mathcal{M} &\rightarrow T_p \mathcal{M} \\ x &\mapsto (x - p)^\perp \end{aligned} \quad (3.1)$$

Then ν_p induces a distribution on $T_p \mathcal{M}$, denoted by Π^\perp . For any Borel set $B \subset T_p \mathcal{M}$, $\Pi^\perp(B) = \Pi(\nu_p^{-1}(B))$. Fix an orthonormal basis for $T_p \mathcal{M}$. The coefficients of $\Delta \mathbf{r}_p^\perp$ and $\Delta \mathbf{n}_p^\perp$ with respect to the orthonormal basis define random variables $\mathbf{X}_p, \mathbf{Y}_p, \mathbf{Z}_p$ and \mathbf{W}_p . Consider the following optimization problem

$$\arg \min_{G_p \in \mathbb{R}^{2 \times 2}} \mathbb{E}_{x \sim \Pi^\perp} \|[Z_p, \mathbf{W}_p] - [\mathbf{X}_p, \mathbf{Y}_p] G_p\|^2. \quad (3.2)$$

Let $\mathbf{\Omega}_p$ and $\mathbf{\Theta}_p$ denote the following random matrices

$$\mathbf{\Omega}_p = \begin{bmatrix} \mathbf{X}_p^2 & \mathbf{X}_p \mathbf{Y}_p \\ \mathbf{X}_p \mathbf{Y}_p & \mathbf{Y}_p^2 \end{bmatrix}, \mathbf{\Theta}_p = \begin{bmatrix} \mathbf{X}_p \mathbf{Z}_p & \mathbf{X}_p \mathbf{W}_p \\ \mathbf{Y}_p \mathbf{Z}_p & \mathbf{Y}_p \mathbf{W}_p \end{bmatrix}. \quad (3.3)$$

Write \mathbb{E}_x for $\mathbb{E}_{x \sim \Pi^\perp}$. The objective function in 3.2 is convex with the following closed form solution

$$G_p = (\mathbb{E}_x \mathbf{\Omega}_p)^{-1} \mathbb{E}_x \mathbf{\Theta}_p. \quad (3.4)$$

Here $\mathbb{E}_x \mathbf{\Omega}_p$ is assumed to be invertible. We will explain this assumption later. In practice, the distribution is unknown hence the expectation cannot be calculated. Instead, we have $(x_p^i, y_p^i, z_p^i, w_p^i), i = 1, 2, \dots, k$, i.i.d. samples from the random vector $(\mathbf{X}_p, \mathbf{Y}_p, \mathbf{Z}_p, \mathbf{W}_p)$. Set

$$\omega_p^i = \begin{bmatrix} (x_p^i)^2 & x_p^i y_p^i \\ x_p^i y_p^i & (y_p^i)^2 \end{bmatrix}, \theta_p^i = \begin{bmatrix} x_p^i z_p^i & x_p^i w_p^i \\ y_p^i z_p^i & y_p^i w_p^i \end{bmatrix}. \quad (3.5)$$

Let $\omega_p = \frac{1}{k} \sum_{i=1}^k \omega_p^i$ be the sample mean of ω_p^i 's, and $\theta_p = \frac{1}{k} \sum_{i=1}^k \theta_p^i$ be the sample mean of θ_p^i 's. The empirical solution is given by

$$\hat{G}_p = \omega_p^{-1} \theta_p. \quad (3.6)$$

Let $[\Psi_p^1, \Psi_p^2]$ be the error term in (3.2). That is,

$$[\mathbf{Z}_p, \mathbf{W}_p] = [\mathbf{X}_p, \mathbf{Y}_p] G_p^* + [\Psi_p^1, \Psi_p^2], \quad (3.7)$$

where G_p^* is the true matrix representing the tangent of Gauss map. Set

$$\mathbf{\Lambda}_p = \begin{bmatrix} \mathbf{X}_p \Psi_p^1 & \mathbf{X}_p \Psi_p^2 \\ \mathbf{Y}_p \Psi_p^1 & \mathbf{Y}_p \Psi_p^2 \end{bmatrix}. \quad (3.8)$$

Thus the true solution is given by

$$G_p^* = (\mathbb{E}_x \mathbf{\Omega}_p)^{-1} (\mathbb{E}_x \mathbf{\Theta}_p - \mathbb{E}_x \mathbf{\Lambda}_p). \quad (3.9)$$

Then we can analyze the following estimation error

$$\text{MSE} = \mathbb{E}_{p \sim \Pi, x \sim \Pi^\perp} \|G_p^* - \hat{G}_p\|_F^2. \quad (3.10)$$

The estimation for mean square error splits into the estimation for bias and variance, that is:

$$\text{MSE} \leq 2 \underbrace{(\mathbb{E}_{p \sim \Pi} \|G_p - G_p^*\|_F^2)}_{\text{Bias}} + \underbrace{(\mathbb{E}_{p \sim \Pi, x \sim \Pi^\perp} \|G_p - \hat{G}_p\|_F^2)}_{\text{Var}}.$$

3.2 Assumptions

We make some general assumptions for the following discussion. The surface \mathcal{M} is assumed to be compact. Therefore, the random variables $\mathbf{X}_p, \mathbf{Y}_p, \mathbf{Z}_p$ and \mathbf{W}_p are bounded. Suppose P_1, P_2, \dots, P_n are i.i.d. samples from Π . Let \mathbf{R}_p be the random variable representing the distance between the origin and its k th nearest neighbor in $\{\nu_p(P_i)\}_{i=1}^n$. According to (2.2), we assume the sum of square $(\Psi_p^1)^2 + (\Psi_p^2)^2$ is bounded by a constant multiple of \mathbf{R}_p^4 . Furthermore, we assume that the absolute value of the correlation coefficient $\rho_{\mathbf{X}_p \mathbf{Y}_p} = \text{cov}(\mathbf{X}_p, \mathbf{Y}_p) / \sqrt{\text{Var} \mathbf{X}_p \text{Var} \mathbf{Y}_p}$ is strictly less than 1. This implies that the matrix $\mathbb{E}_x \mathbf{\Omega}_p$ to be positive definite. In fact, $|\rho_{\mathbf{X}_p \mathbf{Y}_p}| < 1$ implies

$$\mathbb{E}_x \mathbf{X}_p^2 \mathbb{E}_x \mathbf{Y}_p^2 - (\mathbb{E}_x \mathbf{X}_p \mathbf{Y}_p)^2 > 0. \quad (3.11)$$

By the compactness of \mathcal{M} , we can assume the determinant $\det(\mathbb{E}_x \mathbf{\Omega}_p)$ has a strictly positive lower bound.

The condition $|\rho_{\mathbf{X}_p \mathbf{Y}_p}| < 1$ can be explained as follows. Since $|\rho_{\mathbf{X}_p \mathbf{Y}_p}| = 1$ is equivalent to that \mathbf{Y}_p is a linear function of \mathbf{X}_p , we make our assumption to avoid the degeneracy to a one dimensional submanifold. For the same reason we assume $\det(\omega_p)$ is bounded below by $c_k \geq 0$ where the nonnegative sequence $\{c_k\}$ is such that $\lim_{k \rightarrow \infty} c_k > 0$. This implies $\det(\omega_p)$ is strictly positive for sufficient large k .

In summary, we assume the following assertions.

- A.1** The random variables $\mathbf{X}_p, \mathbf{Y}_p, \mathbf{Z}_p$ and \mathbf{W}_p are bounded by global constants.
- A.2** $(\Psi_p^1)^2 + (\Psi_p^2)^2$ is bounded by $C_r \mathbf{R}_p^4$ where $C_r > 0$ is a constant independent of p .
- A.3** The determinant $\det(\mathbb{E}_x \mathbf{\Omega}_p)$ is bounded below by a global constant, and $\det(\omega_p)$ is bounded below by c_k where $\lim_{k \rightarrow \infty} c_k > 0$.

3.3 Bias

To avoid the abuse of notations, we use \mathcal{C} to represent all the constants independent of p . The following lemma gives the bound of the bias term.

Lemma 1. *Under the assumptions A.1 ~ A.3, the following inequality holds*

$$\text{Bias} = \mathbb{E}_x \|G_p - G_p^*\|_F^2 \leq O\left(\frac{k}{n}\right)^2. \quad (3.12)$$

Proof. From the assumption A.2,

$$\begin{aligned} \text{Bias} &\leq \mathbb{E}_{p \sim \Pi} (\|\mathbb{E}_x \mathbf{\Omega}_p\|_F^{-1} \|\mathbb{E}_x \mathbf{\Lambda}_p\|_F^2) \\ &\leq \mathbb{E}_{p \sim \Pi} (\|\mathbb{E}_x \mathbf{\Omega}_p\|_F^{-1} \|\mathbb{E}_x (C_r (\mathbf{X}_p^2 + \mathbf{Y}_p^2) \mathbf{R}_p^4)\|_F). \end{aligned} \quad (3.13)$$

By Cauchy inequality, $\mathbb{E}_x ((\mathbf{X}_p^2 + \mathbf{Y}_p^2) \mathbf{R}_p^4) \leq \sqrt{\mathbb{E}_x (\mathbf{X}_p^2 + \mathbf{Y}_p^2)^2 \mathbb{E}_x \mathbf{R}_p^8}$. From [16], the moments of \mathbf{R}_p is given by

$$\mathbb{E}_x R_p^8 = n \binom{n-1}{k-1} \int_0^1 (Ct^4 + o(t^4)) t^{k-1} (1-t)^{n-k} dt. \quad (3.14)$$

Let $B(p, q) = \int_0^1 t^{p-1} (1-t)^{q-1} dt$ be the Beta function. When p and q are positive integers, we have

$$B(p, q) = \frac{(p-1)!(q-1)!}{(p+q-1)!} = \frac{1}{q \binom{p+q-1}{p-1}}. \quad (3.15)$$

Therefore, (3.14) has the following estimation

$$\begin{aligned}
\mathbb{E}_x R_p^8 &\leq \mathcal{C} n \binom{n-1}{k-1} B(4+k, n-k+1) \\
&\leq \mathcal{C} \frac{n \binom{n-1}{k-1}}{(n-k+1) \binom{n+4}{k+3}} \\
&= \mathcal{C} \frac{(k+3)(k+2)(k+1)k}{(n+4)(n+3)(n+2)(n+1)} = O\left(\frac{k^4}{n^4}\right)
\end{aligned} \tag{3.16}$$

From the assumptions **A.1** and **A.3** we see that the quantities $\|(\mathbb{E}_x \mathbf{\Omega})^{-1}\|_F^2$ and $\mathbb{E}_x(\mathbf{X}_p^2 + \mathbf{Y}_p^2)^2$ are bounded above by global constants. Hence, we obtain (3.12). \square

3.4 Variance

The bound of the variance term is more complicated than the bias term. Firstly we let $\text{Var}_x \mathbf{\Omega}_p$ denote the matrix $\begin{bmatrix} \text{Var}_x \mathbf{X}_p^2 & \text{Var}_x \mathbf{X}_p \mathbf{Y}_p \\ \text{Var}_x \mathbf{X}_p \mathbf{Y}_p & \text{Var}_x \mathbf{Y}_p^2 \end{bmatrix}$.

Lemma 2. *The following inequality holds*

$$\mathbb{E}_x(\det(\omega_p) - \det(\mathbb{E}_x \mathbf{\Omega}_p))^2 \leq O\left(\frac{1}{k}\right). \tag{3.17}$$

Proof. For simplicity, write

$$\begin{aligned}
\det(\mathbb{E}_x \mathbf{\Omega}_p) &= \begin{vmatrix} \mathbf{X}_p^2 & \mathbf{X}_p \mathbf{Y}_p \\ \mathbf{X}_p \mathbf{Y}_p & \mathbf{Y}_p^2 \end{vmatrix} := \begin{vmatrix} D & E \\ E & F \end{vmatrix}, \\
\det(\omega_p) &= \begin{vmatrix} \frac{\sum_{i=1}^k (x_p^i)^2}{k} & \frac{\sum_{i=1}^k x_p^i y_p^i}{k} \\ \frac{\sum_{i=1}^k x_p^i y_p^i}{k} & \frac{\sum_{i=1}^k (y_p^i)^2}{k} \end{vmatrix} := \begin{vmatrix} \hat{D} & \hat{E} \\ \hat{E} & \hat{F} \end{vmatrix}.
\end{aligned} \tag{3.18}$$

By assumption **A.1**, the elements in $\det(\mathbb{E}_x \mathbf{\Omega}_p)$ and $\det(\omega_p)$ are bounded. By Cauchy inequality we have

$$\begin{aligned}
&(\det(\omega_p + \epsilon I) - \det(\mathbb{E}_x \mathbf{\Omega}_p))^2 \\
&\leq 3(\hat{D}^2(\hat{F} - F)^2 + F^2(\hat{D} - D)^2 + (\hat{E} - E)^2(\hat{E} + E)^2) \\
&\leq \mathcal{C}((\hat{F} - F)^2 + (\hat{D} - D)^2 + (\hat{E} - E)^2).
\end{aligned} \tag{3.19}$$

Taking expectation on both sides, we have

$$\begin{aligned}
&\mathbb{E}_x(\det(\omega_p) - \det(\mathbb{E}_x \mathbf{\Omega}_p))^2 \\
&\leq \mathcal{C} \frac{1}{k} (\text{Var}_x \mathbf{X}_p^2 + \text{Var}_x \mathbf{X}_p \mathbf{Y}_p + \text{Var}_x \mathbf{Y}_p^2) \leq O\left(\frac{1}{k}\right).
\end{aligned} \tag{3.20}$$

Therefore, we obtain (3.17). \square

Lemma 3. *There exists $L \in \mathbb{N}$ such that for $k > L$ the following inequality holds*

$$\mathbb{E}_x \|(\omega_p)^{-1} - (\mathbb{E}_x \mathbf{\Omega}_p)^{-1}\|_F^2 \leq O\left(\frac{1}{k}\right). \quad (3.21)$$

Proof. Using the notations defined in 3.17, the inverses of ω_p and $\mathbb{E}_x \mathbf{\Omega}_p$ are given by

$$\begin{aligned} (\omega_p)^{-1} &= \frac{1}{\det(\omega_p)} \begin{bmatrix} \hat{F} & -\hat{E} \\ -\hat{E} & \hat{D} \end{bmatrix}, \\ (\mathbb{E}_x \mathbf{\Omega}_p)^{-1} &= \frac{1}{\det(\mathbb{E}_x \mathbf{\Omega}_p)} \begin{bmatrix} F & -E \\ -E & D \end{bmatrix}. \end{aligned} \quad (3.22)$$

Note that

$$\begin{aligned} \mathbb{E}_x \|(\omega_p)^{-1} - (\mathbb{E}_x \mathbf{\Omega}_p)^{-1}\|_F^2 &\leq 2\mathbb{E}_x \|(\omega)^{-1} - \frac{\det(\mathbb{E}_x \mathbf{\Omega}_p)}{\det(\omega_p)} (\mathbb{E}_x \mathbf{\Omega}_p)^{-1}\|_F^2 \\ &\quad + 2\mathbb{E}_x \|(1 - \frac{\det(\mathbb{E}_x \mathbf{\Omega}_p)}{\det(\omega_p)}) (\mathbb{E}_x \mathbf{\Omega}_p)^{-1}\|_F^2. \end{aligned} \quad (3.23)$$

By assumption **A.3**, there exists $L \in \mathbb{N}$ such that for $k > L$ the determinant $\det(\omega_p)$ is bounded below by a constant $\mathcal{C} > 0$. Therefore,

$$\begin{aligned} &\mathbb{E}_x \|(\omega)^{-1} - \frac{\det(\mathbb{E}_x \mathbf{\Omega}_p)}{\det(\omega_p)} (\mathbb{E}_x \mathbf{\Omega}_p)^{-1}\|_F^2 \\ &\leq \mathcal{C} \mathbb{E}_x ((\hat{F} - F)^2 + (\hat{D} - D)^2 + 2(\hat{E} - E)^2) \\ &\leq \mathcal{C} \left(\frac{1}{k} (\text{Var}_x \mathbf{Y}_p^2 + 2\text{Var}_x \mathbf{X}_p \mathbf{Y}_p + \text{Var}_x \mathbf{X}_p^2) \right) \leq O\left(\frac{1}{k}\right). \end{aligned} \quad (3.24)$$

This gives the bound for the first term. For the second term, by assumption **A.1**, $\|(\mathbb{E}_x \mathbf{\Omega}_p)^{-1}\|_F^2$ is bounded by a constant. Combining (3.17) we see that the second term is bounded by $O\left(\frac{1}{k}\right)$. Hence we obtain the estimation (3.21). \square

Lemma 4. *There exists $L \in \mathbb{N}$ such that for $k > L$, the variance is bounded by the following quantity*

$$\text{Var} \leq O\left(\frac{1}{k}\right). \quad (3.25)$$

Proof. Note that

$$\begin{aligned} \text{Var} &\leq 2\mathbb{E}_{p \sim \Pi, x \sim \Pi^\perp} \|(\mathbb{E}_x \mathbf{\Omega}_p)^{-1} \mathbb{E}_x \mathbf{\Theta}_p - (\omega)^{-1} \mathbb{E}_x \mathbf{\Theta}_p\|_F^2 \\ &\quad + 2\mathbb{E}_{p \sim \Pi, x \sim \Pi^\perp} \|(\omega_p)^{-1} \mathbb{E}_x \mathbf{\Theta}_p - (\omega_p)^{-1} \theta_p\|_F^2. \end{aligned} \quad (3.26)$$

By lemma 3, there exists $L \in \mathbb{N}$ such that for $k > L$ the first term is bounded by $O\left(\frac{1}{k}\right)$. For the second term, since $\|(\omega_p)^{-1}\|_F^2 \leq \mathcal{C}$ for $k > L$, and $\mathbb{E}_x \|\mathbb{E}_x \mathbf{\Theta}_p - \theta_p\|_F^2 \leq O\left(\frac{1}{k}\right)$, it is bounded by $O\left(\frac{1}{k}\right)$. Therefore, we obtain (3.25). \square

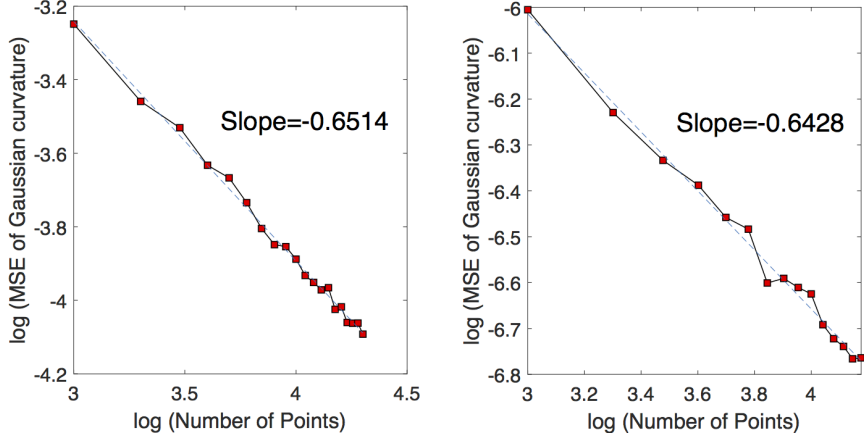


Figure 1: The $\log(n)$ - $\log(\text{MSE})$ plot for torus and ellipsoid. Slopes match the convergence rate.

3.5 Mean Square Error

Combining Lemma 1 and Lemma 4, we have the desired inequality.

Theorem. *Under the assumptions A.1 ~ A.3, there exists $L \in \mathbb{N}$ such that for $k > L$ the following inequality holds*

$$\text{MSE} \leq O\left(\frac{k^2}{n^2}\right) + O\left(\frac{1}{k}\right). \quad (3.27)$$

Therefore the convergence rate is $O(n^{-2/3})$ when k is chosen to be $O(n^{2/3})$.

4 Numerical Experiments

4.1 Convergence Rate

We test the optimal convergence rate on a torus and an ellipsoid. The sample size for the torus with major radius 5 and minor radius 2 ranges from 1000 to 20000. The sample size for the ellipsoid with length of principal axes 6, 6, 8 ranges from 7000 to 30000. k is chosen to be $n^{2/3}$. Figure 1 is the $\log(n)$ - $\log(\text{MSE})$ plot. The slopes match the optimal convergence rate.

4.2 Comparison with Quadratic Fitting

We compare our method with a local quadratic surface fitting method. This is chosen for two reasons. On one hand, quadratic fitting is a commonly used method. Other complicated fitting algorithms involve extra scaling parameters which are difficult to tune in practice. On the other hand, quadratic fitting is studied by many scientists. In

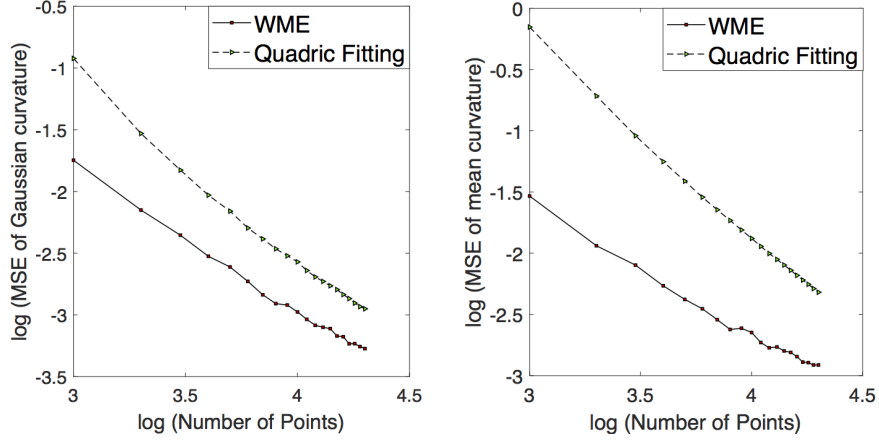


Figure 2: MSE of Gaussian curvature and mean curvature on the torus obtained by WME and quadratic fitting

[17], the authors compared five methods in computing Gaussian and mean curvature for triangular meshes of 2 dimensional surfaces. The result turns out that quadratic fitting excels other methods in computing mean curvature.

The method of quadratic surface fitting is illustrated as follows. First translate and rotate the k -nearest neighbors of a point so that its normal vector coincides with z -axis. Then fit the paraboloid $z = ax^2 + bxy + cy^2$ by least square. The Gaussian curvature and mean curvature at origin P are given by

$$K = 4ac - b^2, H = a + c. \quad (4.1)$$

The MSE of Gaussian curvature and mean curvature are compared as follows. We sample 1000, 2000, \dots , 20000 points on a torus with major radius 5 and minor radius 2. The number of k -nearest neighbors is set to be 100 for each iteration. The time of each computation is also recorded. The result in Figure 2 shows that our method excels the quadratic fitting method without introducing any computational complexity.

The robustness is compared as follows. Again we sample 1000, 2000, \dots , 20000 points on the same torus with multivariate Gaussian noise with zero mean and covariance $\sigma^2 I_3$ where $\sigma^2 \in \{0.01, 0.05, 0.001\}$. The MSE of Gaussian curvature and mean curvature for different noises in Figure 3 show that our method is more robust.

5 Applications

We apply our WME algorithm to real data sets. In practice, point clouds are rarely oriented. We should estimate a unit normal vector field first. The normal vector at P can be computed by applying Principle Component Analysis (PCA) to its k -nearest neighbors [10] and the convergence has been proved by [22]. Note that Gaussian curvature and absolute mean curvature are independent of orientation. Unlike [10], we do not need

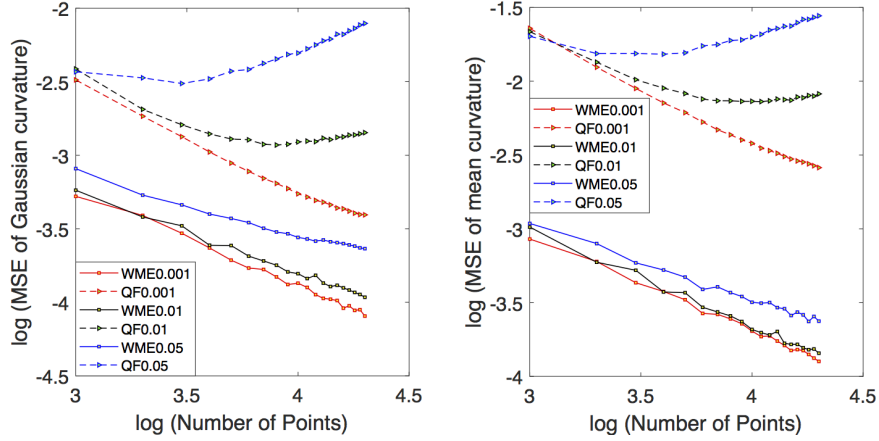


Figure 3: Robustness comparison on the noisy torus. Left and right plots are comparisons of Gaussian and mean curvature respectively.

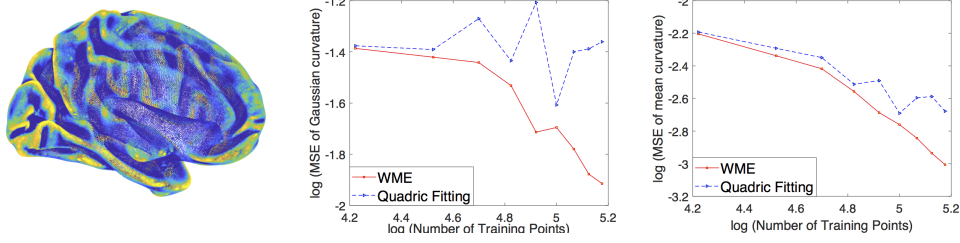


Figure 4: The first panel is the cortical surface data colored by the Gaussian curvature. The last two plots are $\log(\text{MSE})$ of the Gaussian and the mean curvature on this dataset

to apply the Minimal Spanning Tree (MST) algorithm to obtain a global orientation. Instead, a local orientation is enough for computing curvature. Fix a normal vector N at P . Let P_1, P_2, \dots, P_k be k -nearest neighbors of P . The normal vector N_i at P_i is kept if $N_i \cdot N \geq 0$ and flipped if $N_i \cdot N < 0$. Hence we obtain a local orientation. Though we assume the existence of outward/inward normal in error estimation, the results of following experiments show that our algorithm is also practical for arbitrary point clouds.

5.1 Brain Cortical Surface Data

To further illustrate the robustness, we test our method on the real brain cortical surface data. A point cloud of left brain cortical surface is obtained from Human Connectome Projects ([s3://hcp-openaccess/HCP_1200/100206/MNINonLinear/Native/](https://hcp-openaccess.org/HCP_1200/100206/MNINonLinear/Native/)), consisting of 166,737 position vectors. This data is noisy and there is no information about the true curvature of the surface so there is no ground truth and the error can't be calculated. Instead we propose an indirect way to evaluate the performance. Firstly, we estimate the Gaussian and mean curvature for the point cloud based on the entire

dataset. The results are regarded as the true curvature for the underlying cortical surface. Then, the data is divided into training and testing sets. We recalculate the Gaussian and mean curvature for training data. For each testing data, the curvature is inferred to be the mean of curvature for its k nearest neighbors in training data. Finally, we compute the mean square error of the curvature for testing data. The same procedure is also carried out using quadratic surface fitting method. From Figure 4, the mean square error obtained from WME is monotonically decreasing as the number of testing data increases but the error from quadratic surface fitting method is fluctuating, which means that WME is more robust on this real and complicated dataset.

5.2 Point Cloud Simplification

Point clouds are often converted into a continuous surface representation such as polygonal meshes and splines. This process is called surface reconstruction [2]. The reconstruction algorithms require large amounts of memory and do not scale well with data size. Hence before further processed, the complexity of point cloud data should be reduced first. In [24], the authors proposed three types of simplification algorithms: clustering methods, iterative simplification and particle simulation. These methods are based on a quantity defined by the covariance of local data. As claimed by [24], this quantity reflects the curving of point cloud. However, the clear relation between this quantity and the curvatures needs to be further studied. Here we propose a curvature-adaptive clustering simplification algorithm and compare with uniform clustering simplification algorithm.

The uniform clustering method is described as follows. Starting from a random seed point, a cluster C_0 is built by successively adding the nearest neighbors. The process is terminated when the size of cluster reaches the previously set threshold. The next cluster C_1 is built in the same procedure with all points in C_0 excluded. Each cluster is represented by its mean as a representative. The simplified point cloud is given by the representatives.

Intuitively, to preserve the geometric details of point cloud, the points in highly curved region should be kept. Therefore, a seed point with larger curvature should generate smaller cluster. Let Ω represent any kind of (Gaussian, mean or principal) curvature. Suppose $|\Omega|_{\max}$ is the largest absolute curvature of the entire surface. Starting from a random seed point p , with absolute curvature $|\Omega|_p$, a cluster C_p is built by successively adding the nearest neighbors. The process is terminated when the size of cluster reaches

$$\#C_p = \lceil (1 - c \frac{|\Omega_p|}{|\Omega|_{\max}})T \rceil, \quad (5.1)$$

where $0 < c < 1$ is the scaling constant and T is the preset threshold. $\lceil \cdot \rceil$ denotes the ceiling function. The cluster and its curvature are represented by the mean of its points and mean of corresponding curvature. This yields a non-uniform clustering method.

The algorithms are applied to three scanned data sets: the Duke dragon, the Stanford bunny and the Armadillo. Here we adopt absolute mean curvature for curvature-based simplification. After simplification, we apply the Moving Least Square (MLS) method for surface reconstruction [2]. The visualized surfaces in Figure 5, 6 and 7 give a

direct comparison of two algorithms, where the first row corresponds to the uniform simplification while the second row is the curvature-adaptive simplification. Results show that WME preserves more geometric information than the uniform method, especially for the region with larger curvature.

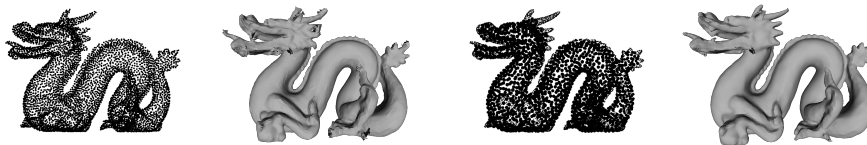


Figure 5: Duke Dragon dataset. The surfaces are reconstructed from 6500 points

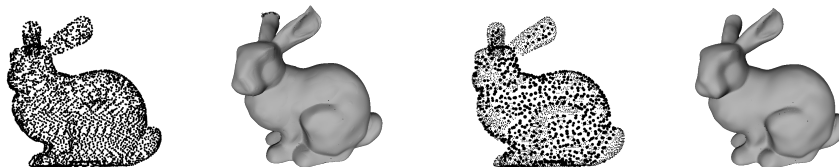


Figure 6: Stanford Bunny dataset. The surfaces are reconstructed from 4400 points.

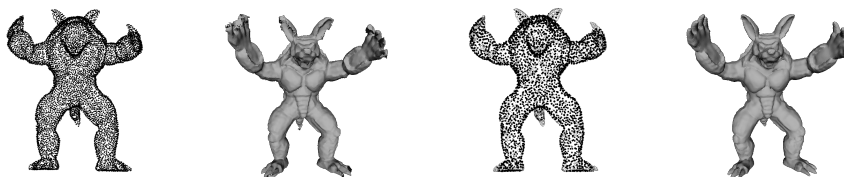


Figure 7: Armadillo dataset. The surfaces are reconstructed from 7800 points

6 Generalizations and Future Works

Our algorithm can be generalized to hypersurfaces in Euclidean spaces of arbitrary dimension without any modification. A hypersurface \mathcal{M} is an m -dimensional manifold embedded in \mathbb{R}^{m+1} . If \mathcal{M} is orientable, then there is a globally defined outward or inward unit normal vector field. Gauss map sends each point to its unit normal vector. The tangent map is also a self-adjoint operator on $T_p\mathcal{M}$. The determinant of this operator is called Gauss-Kronecker curvature.

For manifolds embedded in Euclidean spaces with codimension greater than 1, our algorithm does not hold. Note that the orthogonal complement of the tangent space at each point is a vector space with dimension greater than 1. Therefore, the unit normal vectors are not uniquely determined. To define Gauss map, we should consider a more

abstract space called Grassmannian [20]. Suppose \mathcal{M} is m -dimensional and is embedded in \mathbb{R}^{m+l} . The Grassmannian $\mathbb{G}(m, l)$ is a compact manifold consisting of all l -dimensional linear subspaces in \mathbb{R}^{m+l} . The generalized Gauss map sends each point to its normal space which is a point in $\mathbb{G}(m, l)$. However, the tangent map is not a self-adjoint operator on $T_p\mathcal{M}$. It is a linear map from an m -dimensional vector space to an ml -dimensional vector space. Therefore, to investigate the property of generalized Gauss map we should develop more techniques.

In addition, our method may have applications in many other fields, for example, manifold learning, pattern recognition, medical imaging, etc. Furthermore, as we pointed out, the generalization to high dimensions needs more techniques. It is an interesting yet difficult problem to compute the curvature of points sampled from high dimensional manifolds.

References

- [1] N. Amenta and M. Bern. Surface reconstruction by voronoi filtering. *Discrete & Computational Geometry*, 22(4):481–504, 12 1999.
- [2] M. Berger, A. Tagliasacchi, M. S. Lee, P. Alliez, G. Guennebaud, J. A. Levine, A. Sharf, and C. T. Silva. A survey of surface reconstruction from point clouds. *Computer Graphics Forum*, 36(1):301–329, 2016.
- [3] J. Berkmann and T. Caelli. Computation of surface geometry and segmentation using covariance techniques. *IEEE Transactions on Pattern Analysis and Machine Intelligence*, 16(11):1114–1116, 1994.
- [4] T. K. Dey, J. Giesen, S. Goswami, and W. Zhao. Shape dimension and approximation from samples. *Discrete & Computational Geometry*, 29(3):419–434, 2 2003.
- [5] M. P. do Carmo. *Differential geometry of curves and surfaces*. Prentice-Hall, Englewood Cliffs, N.J., 1976.
- [6] N. Dyn, K. Hormann, S. J. Kim, and D. Levin. Optimizing 3d triangulations using discrete curvature analysis. pages 135– 146, 2000.
- [7] S. Fleishman, D. Cohen-Or, and C. T. Silva. Robust moving least-squares fitting with sharp features. *ACM Trans. Graph.*, 24(3):544–552, 7 2005.
- [8] G. Golub and C. V. Loan. *Matrix Computations*. John Hopkins University Press, Baltimore, 1996.
- [9] R. Hoffman and A. K. Jain. Segmentation and classification of range images. *IEEE Transactions on Pattern Analysis and Machine Intelligence*, PAMI-9(5):608–620, 9 1987.

- [10] H. Hoppe, T. DeRose, T. Duchamp, J. McDonald, and W. Stuetzle. Surface reconstruction from unorganized points. *SIGGRAPH Comput. Graph.*, 26(2):71–78, 7 1992.
- [11] J. B. Huang and C. H. Menq. Automatic data segmentation for geometric feature extraction from unorganized 3-d coordinate points. *IEEE Transactions on Robotics and Automation*, 17(3):268–279, 2001.
- [12] S. J. Kim, C. H. Kim, and D. Levin. Surface simplification using a discrete curvature norm. *Computers & Graphics*, 26(5):657 – 663, 2002.
- [13] C. Lange and K. Polthier. Anisotropic smoothing of point sets. *Computer Aided Geometric Design*, 22(7):680–692, 2005.
- [14] S. G. Lee, F. Zou, and F. A. Wright. Convergence and prediction of principal component scores in high-dimensional settings. *The Annals of Statistics*, 38(6):3605–3629, 2010.
- [15] D. Levin. The approximation power of moving least-squares. *Mathematics of Computation*, 67(224):1517–1531, 1998.
- [16] Y. P. Mack and M. Rosenblatt. Multivariate k-nearest neighbor density estimates. *Journal of Multivariate Analysis*, 9(1):1 –15, 1979.
- [17] E. Magid, O. Soldea, and E. Rivlin. A comparison of gaussian and mean curvature estimation methods on triangular meshes of range image data. *Computer Vision and Image Understanding*, 107(3):139 – 159, 2007.
- [18] D.S. Meek and D.J. Walton. On surface normal and gaussian curvature approximations given data sampled from a smooth surface. *Computer-Aided Geometric Design*, 17(6):521 – 543, 2000.
- [19] Q. Mérigot, M. Ovsjanikov, and L. J. Guibas. Voronoi-based curvature and feature estimation from point clouds. *IEEE Transactions on Visualization and Computer Graphics*, 17(6):743–756, 2011.
- [20] J. W. Milnor and J. D. Stasheff. *Characteristic classes*. Annals of Mathematics Studies. Princeton University Press, Princeton, N.J., 1974.
- [21] M. J. Milroy, C. Bradley, and G. W. Vickers. Segmentation of a wrap-around model using an active contour. *Computer-Aided Design*, 29:299–320, 4 1997.
- [22] N. J. Mitra, A. Nguyen, and L. Guibas. Estimating surface normals in noisy point cloud data. *International Journal of Computational Geometry & Applications*, 14(4-5):261–276, 2004.
- [23] D. S. OuYang and H. Y. Feng. On the normal vector estimation for point cloud data from smooth surfaces. *Computer-Aided Design*, 37(10):1071–1079, 2005.

- [24] M. Pauly, M. Gross, and L. P. Kobbelt. Efficient simplification of point-sampled surfaces. pages 163–170, 10 2002.
- [25] T. Rabbani, F. A. Van Den Heuvel, and G. Vosselmann. Segmentation of point clouds using smoothness constraint. *International Archives of Photogrammetry, Remote Sensing and Spatial Information Sciences*, 36(5):248–253, 2006.
- [26] C. R. Rao. *Linear models and generalizations : least squares and alternatives*. Springer Series in Statistics. Springer, Berlin ; New York, 3rd extended edition, 2008.
- [27] S. Rusinkiewicz. Estimating curvatures and their derivatives on triangle meshes. pages 486–493, 2004.
- [28] P. T. Sander and S. W. Zucker. Inferring surface trace and differential structure from 3-d images. *IEEE Transactions on Pattern Analysis and Machine Intelligence*, 12(9):833–854, 9 1990.
- [29] E. M. Stokely and S. Y. Wu. Surface parametrization and curvature measurement of arbitrary 3-d objects: five practical methods. *IEEE Transactions on Pattern Analysis and Machine Intelligence*, 14(8):833–840, 8 1992.
- [30] C. K. Tang and G. Medioni. Curvature-augmented tensor voting for shape inference from noisy 3d data. *IEEE Transactions on Pattern Analysis and Machine Intelligence*, 24(6):858–864, 6 2002.
- [31] Y. Z. Tang and J. Q. Feng. Multi-scale surface reconstruction based on a curvature-adaptive signed distance field. *Computers & Graphics*, 70:28 – 38, 2018.
- [32] G. Taubin. Estimating the tensor of curvature of a surface from a polyhedral approximation. pages 902–907, 1995.
- [33] W. P. Wang, H. Pottmann, and Y. Liu. Fitting b-spline curves to point clouds by curvature-based squared distance minimization. *ACM Transactions on Graphics*, 25(2):214–238, 2006.
- [34] H. Woo, E. Kang, S. Y. Wang, and K. H. Lee. A new segmentation method for point cloud data. *International Journal of Machine Tools and Manufacture*, 42(2):167–178, 2002.
- [35] S. M. Yamany and A. A. Farag. Surface signatures: an orientation independent free-form surface representation scheme for the purpose of objects registration and matching. *IEEE Transactions on Pattern Analysis and Machine Intelligence*, 24(8):1105–1120, 8 2002.
- [36] H. Yang and E. Lee. Segmentation of measured point data using a parametric quadric surface approximation. *Computer-Aided Design*, 31:449–457, 1999.
- [37] H. B. Yang. Industrial design applications of surface reconstruction algorithm based on three dimensional point cloud data. 00:178–181, 10 2017.

- [38] T. Y. Yuan, X. B. Peng, and D. D. Zhang. Direct rapid prototyping from point cloud data without surface reconstruction. *Computer-Aided Design and Applications*, 15:1–9, 11 2017.